Proceedings of the 7th IEEE
International Conference on Nanotechnology
August 2 - 5, 2007, Hong Kong

Rapid production of biocompatible polymeric nanoparticles for functionalization via radio-frequency acoustic atomization

James Friend* Leslie Yeo* Dian Arifin* Adam Mechler†

Polymeric nanoparticles are critical to a wide range of emerging applications, including in-vivo drug and gene delivery, amplification of DNA hybridization biosensors, and immunodiagnostics. [1–3] A reliable, reproducible and efficient production method for synthesizing nanoparticles below 200 nm, however, has yet to be devised. [4] The conventional techniques currently employed, which include solvent evaporation/extraction, [5] spray drying, [6] nanoprecipitation, [7] and, emulsion photocrosslinking, [8] typically require multi-step procedures, the use of a considerable amount of solvent, and often result in a wide distribution of particle sizes. Other non-conventional techniques overcome these problems but have troubling drawbacks, as in high voltages for electrospraying [9], for example. In this work we demonstrate the use of surface acoustic wave (SAW) atomization together with a nonuniform evaporation and nucleation process to give sub-50-nm diameter monodisperse nanoparticles. SAW atomization is a straightforward and energy efficient technique to generate relatively homogeneous particle size distributions that can be carried out on a chip-scale microdevice for portable drug delivery applications or scaled up for industrial production. It employs technology originally developed for the entirely different purpose of signal filtering and multiplexing, [10] and provides direct control over the size of the particles through adjustment of the operating frequency of the ultrasonic vibration. [11, 12]

Here the SAW atomization device is a single interdigital transducer (IDT) consisting of 25 pairs of straight electrodes formed of 250 nm aluminum atop a 4 nm titanium layer in a basic full-width interleave configuration sputter-deposited onto a 127.68° Y–x–cut lithium niobate ($LiNbO_3$ or LN, Roditi UK, Ltd., London) single crystal piezoelectric substrate, as schematically depicted in Fig. 1(a). Absorption gel (α-gel, Geltec Ltd., Yokohama, Japan) was used to suppress the leftward SAW from the IDT. The SAW wavelength λ was chosen to be 440 μm, thus specifying the electrode and inter-electrode gaps along the x-axis at 110 μm. The IDT finger width perpendicular to the x-axis is 10 mm with a gap of 1 mm between the electrode ends and opposite bus bar, which has a width of 3 mm. Application of an oscillating electric field matching the designed resonance frequency of 8.611 MHz at a power of 30 W then induces a shallow (3–4λ deep) electroelastic Rayleigh wave [10] along the substrate surface with a displacement of approximately 10 nm, as illustrated in Fig. 1(b).

Using a syringe pump at a flow rate of 24 ml/hr, we maintained a 25 μl droplet of the working fluid on the substrate in the path of the SAW, composed of 1% w/w poly-ε-caprolactone (PCL, Sigma-Aldrich Pty. Ltd., Australia) dissolved in acetone; PCL is a biocompatible and biodegradable polymer which is commonly used for in-vivo controlled release drug delivery. [13] Transmission of acoustic energy into the liquid drop then occurs through leaky SAW, shown in Fig. 1(b), which is the diffraction of the axially-polarized compressional wave component of the SAW into the fluid at the Rayleigh angle, θ_R, defined by the ratio of the bulk wave speeds in the substrate and the fluid; for $LiNbO_3$ and water, the Rayleigh angle is $\theta_R = 23^o$. [12] As the leaky SAW propagates in the fluid, capillary waves are induced at the liquid-air interface due to excitation of lower-order vibration modes at the liquid interfacial membrane. With sufficient power input into the drop such that the acoustic stress overwhelms the capillary stress, desta-

*Drs. Friend, Yeo, and Arifin are with the Micro-Nanophysics Research Laboratory, Monash University, Clayton (Melbourne) VIC 3800 Australia. Corresponding e-mail: james.friend@eng.monash.edu.

†Dr. Mechler is with the School of Chemistry, Monash University.

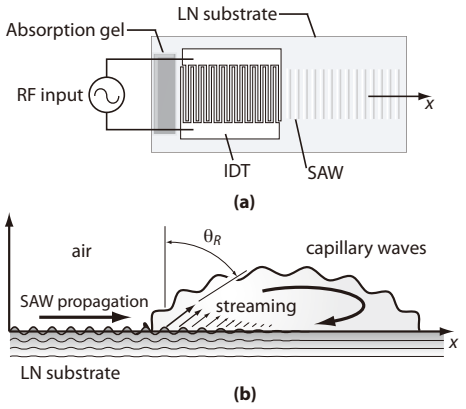

Figure 1: Surface acoustic waves are (a) generated across the LN substrate via an sinusoidal electrical input into the interdigital electrode. Acoustic streaming and subharmonic capillary wave generation (b) occurs in a fluid droplet placed on the substrate as a consequence of interaction with the SAW. The acoustic streaming induces internal recirculation while the oscillatory acoustic field induces the capillary waves.

bilization of the interface occurs resulting in atomization of the liquid, thus producing a fine continuous mist of droplets. As the droplets are ejected, the residual solvent in which the PCL is dissolved evaporates in-flight, leaving behind solid polymer particles. Here, the atomization is carried out at room temperature and 50% relative humidity. For PCL concentrations greater than 1% w/w, a polymer film forms along the substrate surface within a few minutes of operation, reducing the amount of acoustic energy that is allowed to propagate into the drop and therefore reducing atomization efficiency

The PCL solution was first atomized into 50 ml of continuously stirred mixtures of deionized water and surfactant for 20 minutes placed at varying distances from the SAW device. The surfactants used were sodium dodecyl sulphate (SDS) and Tween-20 (both Sigma Aldrich Pty. Ltd., Australia); SDS is a common anionic surfactant and Tween-20 is a non-foaming, non-ionic, biocompatible surfactant. The critical micelle concentrations (CMC) of SDS and Tween-20 are 8.7 mM and 0.06 mM, respectively. Due to the hydrophobic nature of PCL in the surfactant/water mixture, the particles tended to accumulate at the liquid surface, forming large polymer agglomerates. After removing the aggregates from the surface, the suspension was centrifuged at 7000 rpm for 10 minutes. The aliquot was separated and the z-average diameter [14] of the suspended particles was measured using a dynamic light scattering (DLS) device (Zetasizer Nano S, Malvern Instruments Ltd., UK), capable of measuring particle sizes in the range 0.6 nm–6 μm. For each set of system parameters, the atomization procedure and particle size measurement was carried out three times.

The particle sizing results from DLS were confirmed using Transmission Electron Microscopy (TEM) and Atomic Force Microscopy (AFM). In the former, PCL nanoparticles were collected into an agitated 0.1% v/v Tween-20 solution, placed 8 cm below the SAW device, and samples of the solution were placed on a TEM substrate (holey support film, 200 mesh copper grid, ProSciTech, Australia) and subsequently air dried in a covered container. The particles were then imaged using a TEM (Phillips CM20, Royal Phillips Electronics, Australia) with a resolution of 0.27 nm. In the latter, 20 μl of a water/ethanol mixture in which the surfactant-free PCL particles were collected within was pipetted onto atomically flat mica and dried under a nitrogen gas flow for 15 minutes; the addition of ethanol served to prevent rolling of the particles by the AFM tip due to the water acting as a lubricant. [15] The surface morphology was then imaged using a Nanoscope IV Multimode AFM (Veeco, USA) in tapping mode, using Mikro-Masch NSC15 probes at resonant frequencies of approximately 300 kHz.

The z-average diameters of the nanoparticles produced by the SAW atomization process and collected in SDS and Tween-20 across varying distances from the SAW device, obtained through the DLS measurements, are tabulated in Table I. The smallest particles (181 ± 4.9 nm) were obtained when collected at a distance 8 cm away from the atomizer in a sonicated 10 mM SDS solution. The size distributions of the nanoparticles collected in the lowest SDS and Tween-20 concentrations are shown in Fig. 2, indicating the particle distributions are both symmetric and monodisperse with either measurement technique. Further, these nanoparticles are noticeably smaller than those generated by a 1.85/5.32 MHz piston atomizer and collected in SDS solutions of similar concentrations. [16] The observed trends also agree with those in Lee *et al.* [17] who noted that the par-

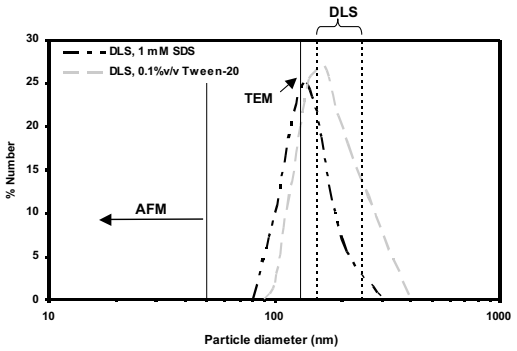

Figure 2: Number percentage size distributions of atomised PCL particles as measured by Dynamic Light Scattering (DLS). TEM and AFM results are included for comparison.

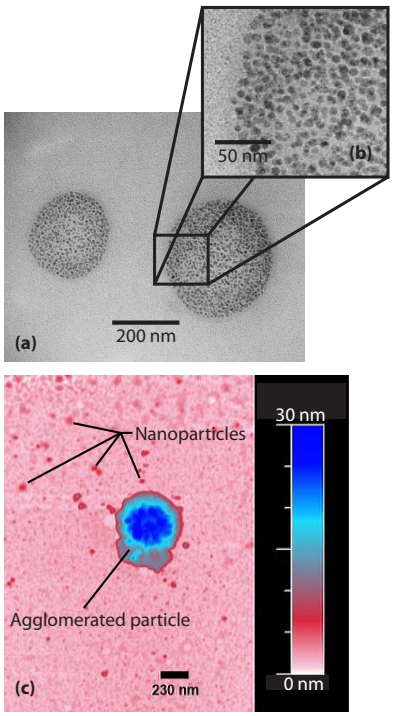

Figure 3: Transmission electron and atomic force microscopy images of the particles formed via SAW atomization and solvent evaporation. The particles (a) under closer observation via TEM (b) appear to be agglomerated, and this is supported by the appearance of the particles (c) under AFM. Note the flattened morphology of the particle in the AFM—only 30 nm in height—and the appearance of many nanoparticles smaller than 50 nm in diameter about this agglomeration. Prior to particle deposition the entire atomically flat mica surface would have appeared white in this image.

ticle size increased with the Tween-20 concentration. However, while we expected to improve the monodispersity of the suspensions by sonicating the collection solution during atomization, we note the opposite result from Table I.

TEM images of the nanoparticles are shown in Fig. 3(a). The average diameter over 21 nanoparticles observed in images like Fig. 3(a) was 131 ± 32 nm. In addition, the particles were observed to be spherical and composed of agglomerations of particles of far smaller diameter, as can be clearly seen by the enlargement in Fig. 3(b), though the morphology of the agglomeration cannot be discerned here using the TEM. The AFM images in Fig. 3(c), on the other hand, shows the surface of the mica covered with spherical nanoparticles with diameters below 50 nm. A larger particle roughly corresponding to the 150 nm order diameters from the DLS measurements and TEM imaging, although flattened either by surface forces or by loss of solvent, can also be observed in Fig. 3(c). Closer inspection of the surface morphology of this larger particle reveals that it consists of an agglomeration of smaller nanoparticles of similar size to those lying adjacent to the particle agglomerate. Similar 150–200 nm diameter agglomerates comprising sub-50 nm particulates are also consistently observed in other TEM scans (not shown).

The observation of 150–200 nm order agglomerates of sub-50 nm particles can be explained through a twofold process. The first consists of the Rayleigh instability mechanism, in which the oscillation at the interface due to the presence of the leaky SAW acoustic field in the drop overwhelms the capillary stress at the interface. Destabilization of the interface causes its break-up to form a fine mist of atomized droplets. The mean droplet diameter was originally estimated from a balance between the capillary and acoustic stresses by Rayleigh in 1883:

$$D \sim \left(\frac{8\pi\gamma}{\rho f^2}\right)^{1/3}, \qquad (1)$$

wherein γ and ρ are the surface tension and the density of the liquid, respectively, and f is the frequency of the acoustic radiation. Although the relationship above was first proposed for the case of bulk ultrasonic vibration, [11] we note that this scaling holds for any generic process in which the dominant forces are the acoustic and capillary stresses. The coefficient in Eq. (1)

differs from the value of 0.34 determined empirically by Lang, [11] but nevertheless remains unit order. Assuming that the interfacial tension and density of the working fluid is close to that of pure acetone at 25°C, i.e., 23.7 mN/m and 0.785 g/ml, respectively, the size of the ejected droplet due to acoustically-driven interfacial destabilization is roughly 1 μm.

We assume that complete evaporation of acetone occurs during the fraction of time that the particles are in-flight, not unreasonable given the simple diffusion-based prediction of the evaporation of a microdroplet of acetone would occur in microseconds and the time of flight is on the order of a second. We note from the DLS measurements in Table I that the particle size *increases* with the distance the particle travels before reaching the collection fluid. However, the particle size does not increase beyond 200 nm as the travel distance is further increased, and this suggests the solvent is indeed completely evaporating. In addition, it is also possible to assume that each droplet, on average, contains 1% w/w PCL (density of 1.15 g/ml), such that the particle volume after complete evaporation of the solvent is roughly 0.68% of the droplet volume. This suggests average particle diameters between 150–200 nm, which is consistent with the DLS and TEM results and the size of the particle agglomerates observed using the AFM.

The appearance of the sub-50 nm particulates that make up the larger particle agglomerates can be explained by a second process that occurs simultaneously during the in-flight evaporation of the solvent. Given that the evaporation occurs at the surface of the ejected droplets, the solute concentration is highest in a thin boundary layer adjacent to the droplet surface. Spatial nonuniformities in the surface evaporative process then result in a thermodynamic instability in which phase separation via spinodal decomposition takes place as a result of the rapid quenching of the temperature. Similar phase separation events are commonly observed in other ejection phenomena. One example is in electrospinning jets, in which the phase separation is responsible for the formation of nanopores on the surface of the fiber. [18–20] In this case, the supercooled-driven phase separation process results in a metastable state in which both solvent-rich and polymer-rich regions exist The latter solidifies much more rapidly than the former thus creating a series of nucleation sites along the surface of the evaporating droplet. The number of these sites is controlled by the solute concentration and solubility.

The above mechanism is corroborated by previous work on PCL-solvent systems. [21, 22] Acetone is known to be a good (hydrophilic) solvent for PCL, having closely matched solubility parameters, [22] and tends to promote intra-aggregation between the PCL molecules. [21] Further, a large number of nucleation sites could be expected to form during rapid evaporation, [23] and as a result, each nucleation site therefore forms a cluster of PCL molecules until a critical size is achieved. Such template-induced crystalline self-assembly driven by solvent evaporation is well-known in colloidal systems. [24]

The critical cluster size can be estimated from classical nucleation theory. Assuming that the properties of each nucleus can be described by bulk properties, the net excess free energy change of a single nucleus with radius R is given by

$$\Delta G_R\left(R\right) = \frac{4}{3}\pi R^3 \Delta G_v + 4\pi\gamma R^2, \qquad (2)$$

where ΔG_v is the driving force for evaporation and γ the surface tension of the nucleus. The critical radius R_c can then be obtained when ΔG_R is a maximum:

$$R_c = \frac{-2\gamma}{\Delta G_v}. \qquad (3)$$

Under supercooled conditions, it is possible to assume that the entropic contribution is small compared to the enthalpy change of vaporization (≈ -540 kJ/kg). For the polymer concentration used, the critical radius is then estimated to be in the order 10 nm, commensurate with the sub-50 nm particulates that comprise the larger 150–200 nm order particle aggregates.

To conclude, we have demonstrated a straightforward and rapid technique for the synthesis of spherical monodispersed polymeric nanoparticles through a continuous operation SAW device. At a resonance frequency of 8.611 MHz, submicron particle assemblies between 150–200 nm were formed due to acoustically-driven atomization via capillary instabilities at the interface of a PCL/solvent drop maintained on the substrate of a SAW device. These large particle aggregates, in turn, are composed of sub-50 nm particles. We attribute these smaller particles to form as a re-

sult of a spatially non-uniform solvent evaporation enhanced nucleate templating process.

Table 1: z-average particle diameters [14] as a function of various process parameters.

[SDS] mM	[Tween-20] % v/v	Distance cm	z-average dia. nm
1	—	8	162.3 ± 3.0
10	—	8	153.4 ± 4.0
40	—	8	185.4 ± 4.5
70	—	8	180.2 ± 13.6
100	—	8	177.1 ± 6.9
—	0.1	8	159.8 ± 1.7
—	1	8	169.9 ± 7.6
—	5	8	247.5 ± 3.5
10	—	6	167.3 ± 5.6
10	—	12	214.6 ± 2.5
10	—	16	236.0 ± 61.0
10*	—	8	181.4 ± 4.9

* The collection solution was sonicated during atomization.

References

[1] Lu, Y.; Chen, S. C. Adv. Drug Del. Rev. **2004**, *56*, 1621–1633.

[2] Wang, J. Anal. Chim. Acta **2003**, *500*, 247–257.

[3] Jain, K. K. Clin. Chim. Acta **2005**, *358*, 37–54.

[4] Cho, E. C.; Cho, K.; Ahn, J. K.; Kim, J.; Chang, I.-S. Biomacromolecules **2006**, *7*, 1679–1685.

[5] Mu, L.; Feng, S. S. J. Controlled Release **2002**, *80*, 33–48.

[6] Hadinoto, K.; Phanapavudhikul, P.; Kewu, Z.; Tan, R. B. H. Ind. Eng. Chem. Res. **2006**, *45*, 3697–3706.

[7] Craparo, E. F.; Cavallaro, G.; Bondì, M. L.; Giammona, G. Macromol. Chem. Phys. **2004**, *205*, 1955–1964.

[8] Zhang, G.; Niu, A.; Peng, S.; Jiang, M.; Tu, Y.; Li, M.; Wu, C. Acc. Chem. Res. **2001**, *34*, 239–256.

[9] Yeo, L. Y.; Gagnon, Z.; Chang, H.-C. Biomaterials **2005**, *26*, 6122–6128.

[10] White, R. M.; Volmer, F. W. Appl. Phys. Lett. **1965**, *7*, 314–316.

[11] Lang, R. J. J. Acoust. Soc. Am. **1962**, *34*, 6–8.

[12] Kurosawa, M.; Watanabe, T.; Futami, A.; Higuchi, T. Sens. Act. A **1995**, *50*, 69–74.

[13] Sinha, V. R.; Bansal, K.; Kaushik, R.; Kumria, R.; Trehan, A. Int. J. Pharm. **2004**, *278*, 1–23.

[14] Bonard, J.-M.; Stora, T.; Salvetat, J.-P.; Maier, F.; Stöckli, T.; Duschl, C., Forró, L., de Heer, W. A.; Châtelain, A. Adv. Mater. **1997**, *9*, 827–831.

[15] Murakami, H.; Kobayashi, M.; Takeuchi, H.; Kawashima, Y. Int. J. Pharm. **1999**, *187*, 143–152.

[16] Forde, G.; Friend, J.; Williamson, T. Appl. Phys. Lett. **2006**, *89*, 064105.

[17] Lee, Y.-G.; Oh, C.; Yoo, S.-K.; Koo, S.-M.; Oh, S.-G. Micropor. Mesopor. Mater. **2005**, *86*, 134–144.

[18] Bognitzki, M.; Czado, W.; Frese, T.; Schaper, A.; Hellwig, M.; Steinhart, M.; Greiner, A.; Wendorff, J. H. Adv. Mater. **2001**, *13*, 70–72.

[19] Kim, G.-M.; Michler, G. H.; Pötschke, P. Polymer **2005**, *46*, 7346–7351.

[20] Yeo, L. Y.; Friend, J. R. J. Exp. Nanosci. **2006**, *1*, 177–209.

[21] Tang, Z. G.; Black, R. A.; Curran, J. M.; Hunt, J. A.; Rhodes, N. P.; Williams, D.F. Biomaterials **2004**, *25*, 4741–4748.

[22] Huang, J. C.; Lin, K. T.; Deanin, R. D. J. Appl. Polym. Sci. **2006**, *100*, 2002–2009.

[23] Leong, K. H. J. Aerosol Sci. **1987**, *18*, 511–524.

[24] Hoogenboom, J. P.; Rétif, C.; de Bres, E.; van de Boer, M.; van Langen-Suurling, A. K.; Romijn, J.; van Blaaderen, A. Nano Lett. **2004**, *4*, 205–208.